On the use of lithogenic tracer measurements in aerosols to constrain dust deposition fluxes to the ocean southeast of Australia.

Claudia Hird [a*], Morgane M.G. Perron [ab*], Thomas M. Holmes [c*], Scott Meyerink [c], Christopher Nielsen [a], Ashley T. Townsend [d], Patrice de Caritat [e], Michal Strzelec [a], Andrew R. Bowie [ac]

a Institute for Marine and Antarctic Studies (IMAS), University of Tasmania, Battery Point, Tasmania, Australia.

b Université de Brest - UMR 6539 CNRS/UBO/IRD/Ifremer, Laboratoire des sciences de l'environnement marin (LEMAR) - Institut Universitaire Européen de la Mer - Rue Dumont D'Urville, 29280 Plouzané, France

c Australian Antarctic Program Partnership (AAPP), University of Tasmania, Battery Point, Tasmania, Australia.

d Central Science Laboratory, University of Tasmania, Hobart, Tasmania, Australia

e John de Laeter Centre, Curtin University, Bentley WA 6845, Australia

* These authors contributed equally to this work.
Correspondence to: Morgane M.G. Perron, morgane.perron@univ-brest.fr

Abstract

1   Australia contributes a significant amount of dust-borne nutrients (including iron) to the Southern
2   Ocean, which can stimulate marine primary productivity. A quantitative assessment of the
3   variability of dust fluxes from Australia to the surrounding ocean is therefore important for
4   investigating the impact of atmospheric deposition on the Southern Ocean's carbon cycle. In this
5   study, lithogenic trace metals (aluminium, iron, thorium and titanium) contained in aerosols
6   collected between 2016 and 2021 from kunanyi/Mount Wellington in lutruwita/Tasmania
7   (Australia) were used to estimate dust deposition fluxes. Lithogenic fluxes were calculated using
8   each tracer individually, as well as an average using all four tracers. This latter approach enabled
9   an assessment of the uncertainty associated with flux calculations using only individual tracers.
10 Elemental ratios confirmed the lithogenic nature of each tracer in aerosols when compared with
11 both Australian soil samples and the average Earth's upper continental crust. Lithogenic flux
12 estimates showed annual dust deposition maxima during the austral summer, following the
13 Australian dust storm season, and annual minimum deposition flux over winter. The data provided

14 here will help to constrain model estimates of southern hemisphere atmospheric deposition fluxes

15 and their subsequent impact on global ocean biogeochemical cycles.

16

17 **Environmental significance / Plain language summary**

18 Dust deposition flux was investigated in lutruwita/Tasmania, Australia, between 2016 and 2021.

19 Results show that the use of direct measurement of aluminium, iron, thorium and titanium in

20 aerosols to estimate average dust deposition fluxes limits biases associated with using single

21 elements. Observations of dust deposition fluxes in the Southern Hemisphere are critical to

22 validate model outputs and better understand the seasonal and interannual impacts of dust

23 deposition on biogeochemical cycles.

1. Introduction

25 Lithogenic mineral particles such as iron oxyhydroxides, kaolinite, illite and smectite are

26 commonly entrained into the atmosphere (Cudahy et al., 2016) following the erosion of the Earth's

27 Upper Continental Crust (UCC) (Crawford et al., 2021). Such dust particles are the primary source

28 of trace metals including aluminium (Al), iron (Fe), thorium (Th) and titanium (Ti) to the

29 atmosphere, which can therefore be used as tracers of aeolian lithogenic inputs to the ocean (Baker

30 et al., 2020). Dust carries important nutrients, including Fe, to marine ecosystems, feeding primary

31 producers (Mackie et al., 2008). Due to the current lack of field observations on the concentrations

32 of aeolian trace metals and their corresponding dust deposition fluxes, large uncertainties remain

33 regarding how and to what extent dust supply fertilises key oceanic regions such as the Southern

34 Ocean with vital nutrients. This leads to a poor understanding of the impact of dust deposition on

35 the biological carbon pump.

36

37 The amount of dust entrained into the atmosphere depends on soil surface roughness, vegetation

38 and coverage, on particle size, composition, and moisture content, and on local conditions such as

39 wind speed and rainfall, which change both regionally and seasonally (Mahowald et al., 2009). Air

40 masses can carry dust over thousands of kilometres before particles return to land or fall onto the

41 surface ocean (Mackie et al., 2008). Atmospheric deposition of dust to the open ocean has been

42 demonstrated to act as a key supplier of vital macro- and micro-nutrients (such as Fe) to the marine

43 ecosystem (Mackie et al., 2008; Weis et al., 2024). For example, during the austral summer 2019-

44 2020, nutrient supply from large dust-containing bushfire emissions (Perron et al., 2022; Hamilton

45 et al., 2022) was identified as the main trigger of a large and long-lasting phytoplankton bloom in

46 the South Pacific Ocean (Weis et al., 2022).

47

48 Field and modelling approaches to estimating dust deposition both offer various benefits and

49 drawbacks. Field observations at sea are influenced by local environmental conditions (i.e.,

50 weather, surface ocean properties) and are not representative of the large scale or long-term

51 atmospheric deposition trends (Anderson et al., 2016). Time-series stations on land can overcome

52 the issue of temporal coverage but may not be representative of atmospheric loading and

53 deposition over remote oceanic regions. To date, global models are not capable of reproducing

54 atmospheric concentrations of trace metals transported in dust to remote areas and cannot

55 accurately quantify particle settling rates (Anderson et al., 2016). Considering the Southern

56 Hemisphere, model estimates tend to overestimate total dust emission at the source and

57 underestimate soluble trace element deposition fluxes over the ocean (Anderson et al., 2016; Ito et

58 al., 2020). To reduce uncertainty in dust deposition fluxes to the open ocean it is essential to

59 validate model fluxes using field-based observations. Long-term atmospheric observatories,

60 particularly near the coasts, are attracting increasing interest from the scientific community as a

61 platform to better understand seasonal to interannual patterns of deposition events in addition to

62 shipboard observations and satellite estimates (Perron et al., 2022; De Deckker, 2019).

63

64 In Australia, the large spatial heterogeneity of soil types and the highly episodic nature of weather

65 events such as droughts, bushfires and dust storms make it particularly difficult to model dust

66 deposition fluxes (Mackie et al., 2008), though modern dust emissions from South Australia have

67 been observed as far as the snow sheet of inner Antarctica (Vecchio et al., 2024). A main source

68 of trace metals to the Australian sector of the Southern Ocean is dust carried from kati thanda/Lake

69 Eyre and dhungala-barka/Murray-Darling geological basins (De Deckker, 2019). The typical dust

70 storm season in Australia spans from September to November (austral spring), with the most

71 extreme storms occurring in September (O'Loingsigh et al., 2017). The dust season can extend

72 through the austral summer due to bushfires (and postfire unvegetated ground) across southern

73 Australia (Hamilton et al., 2022). In a study conducted by Perron et al. (2022), atmospheric

74 concentrations of mineral dust and associated lithogenic tracers (Al, Fe and Ti) were reported to

75   be 2.5-fold higher, on average, during fire events compared to days not impacted by bushfires in

76   lutruwita/Tasmania, Australia.

77

78   Dust deposition fluxes reported by different models range over an order of magnitude (from 0.55

79   to 5.48 mg m^{-2} d^{-1}) over the Southern Ocean region southeast of Australia (Mahowald et al., 2006;

80   Weis et al., 2024). Different methods have also been used to estimate dust deposition fluxes from

81   field samples. While broadly used in air pollution studies (Bindu et al., 2016), total aerosol loading

82   measurements based on gravimetry does not enable the discrimination of atmospheric sources

83   (e.g., dust vs anthropogenic). In addition, such a method is not compatible with atmospheric trace

84   metal studies, where strict protocol requires minimal filter handling to prevent contamination. from

85   the analysis of a single tracer element, for example Al or Th, in aerosol samples and in seawater

86   (Anderson et al., 2016). However, single element dust flux estimates are subject to anomalous data

87   stemming from contamination, deviation from the mean UCC, or preferential mineralization

88   following a particular laboratory protocol. Recently, the analysis of four lithogenic tracers

89   (namely, Al, Fe, Th, and Ti) in marine sinking particles collected at the Southern Ocean Time-

90   Series (SOTS) mooring station (140°E, 47°S) were used to calculate an average 'multi-tracer'

91   estimate of dust deposition fluxes to surface waters of the subantarctic ocean south of Australia

92   (Traill et al., 2022). The latter field-based flux estimates showed good agreement with remotely

93   sensed proxies of dust transport and modelled deposition estimates. Elemental ratio analysis in the

94   same sediment trap samples suggested that lithogenic material from southeastern Australia was

95   the most likely source of Al, Fe, Th and Ti to this area of the Southern Ocean (Traill et al., 2022).

96

97   In this study, the analysis of the same four lithogenic tracers (Al, Fe, Th, and Ti) was performed

98   in aerosol samples collected at the kunanyi/Mount Wellington time-series sampling station in

99   southern lutruwita/Tasmania (Australia). Dust deposition fluxes were estimated from both

100   individual tracer concentrations and using the multi-tracer approach used by Traill et al. (2022).

101   Here we report a 5-year (2016-2021) time-series of dust deposition flux estimates downwind of

102   the south-eastern Australian dust path, at one of the gateways to the Southern Ocean. The

103   suitability of the four metals as lithogenic tracers was also verified by comparing elemental ratios

104   (relative to Al) in the aerosol samples to the average topsoil composition in Australia (this study)

105   and to the averaged UCC composition (McLennan et al., 2001).

106

2. Material and methods

2.1 Aerosol collection and study site

kunanyi/Mount Wellington overlooks Hobart, the capital city of the Australian island state of lutruwita/Tasmania. The mountain is in a strategic position for sampling one of the three major atmospheric pathways in Australia (Baddock et al. 2015; Bowler 1976), where air-masses from mainland Australia are transported south-eastwards over lutruwita/Tasmania (and our sampling site, Figure 1) before reaching the Southern Ocean. This study uses aerosol filters collected on a HiVOL 3000 air particulate sampler (Ecotech, Acoem, Melbourne, Australia) positioned at 1271 m above sea level, on the summit of kunanyi/Mount Wellington. Filter samples have been collected for Total Suspended Particulates (TSP) since September 2016, with each sample representing a period ranging from a few days to 2 weeks, depending on weather conditions and specific weather events, and allowing for sampler servicing and calibration. Samples suspected of contamination or that were significantly wet at the time of recovery were discarded and sampling was suspended in the wintertime of 2017, 2018 and 2019 for operational reasons. As a result, 125 aerosol samples were selected from the kunanyi/Mount Wellington atmospheric time-series collection for this study (November 2016 - February 2022). The origin and concentration of aerosol Fe in 80 samples from this dataset was previously reported in Perron et al. (2022), however the

124 present study differs in using total concentrations of Fe, Al, Th and Ti to calculate atmospheric

125 (dust) deposition fluxes and the associated seasonal and interannual trends at the sampling station.

126

127
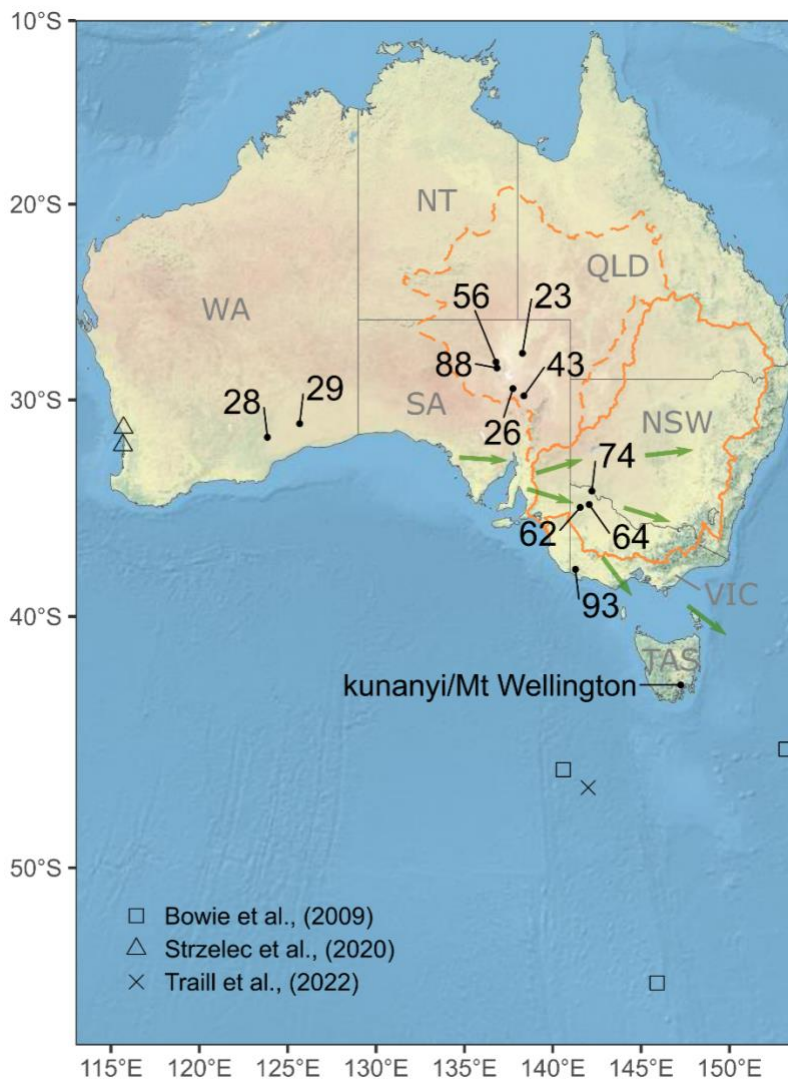
Figure 1. Location of the aerosol sampling station at kunanyi/Mount Wellington in Tasmania (TAS). Black dots display the locations of selected NGSA soil samples in the Australian states of Western Australia (WA), South Australia (SA) and Victoria (VIC) with identification numbers annotated (see Table S2). Prevailing dust pathways of southeast Australia are displayed as green arrows adapted from Sprigg (1982) and Mackie et al. (2008). The kati thanda/Lake Eyre (dashed line) and dhungala-barka/Murray-Darling (solid line) geological basins are delineated in orange. Location of previous field studies that estimated dust deposition fluxes are also indicated.

135

2.2 Aerosol leaching protocol

Laboratory work for aerosol and soil sample processing (sections 2.2 and 2.3) followed

GEOTRACES recommended procedures for ultra-trace sampling and analysis (Cutter et al., 2017).

139   All reagents were ultra-high purity (UHP) and either purchased (Baseline, SeaStar Chemicals) or
140   distilled in-house using instrument quality reagents (IQ grade, SeaStar Chemicals). Whatman W41
141   (203mm x 254mm paper sheets, Sigma-Aldrich) filters were acid washed in a series of 24h
142   hydrochloric acid (0.5 M HCl) baths and rinsed with UHP water to leach any impurities and reduce
143   the impact of the cellulose filter on the analysis of trace elements in aerosols (Perron et al., 2020a).
144   Perron et al. (2020a) suggested a 3-step leaching method to define trace metal concentrations and
145   solubility in aerosols taken from land-based stations in Australia (Strzelec et al., 2020a, 2020b)
146   and on research vessels operating around Australia and in the Southern Ocean (Perron et al., 2020b,
147   2021). Although samples were collected and analysed in batch over several years, the collection
148   and analysis of each batch of samples follow the same protocol and the resulting data was quality-
149   controlled against blanks, replicate analysis and Certified Reference Materials (Table S1).

150

151   One sub-sample of 47mm diameter was cut off each aerosol filter sheet collected at our sampling
152   station using a sharp titanium punch cutter (Perron et al., 2020). Sub-samples were successively
153   leached using UHP water (Milli-Q®, 18.2 MΩ) and 1.1 M ammonium acetate (10 mL, pH 4.7).
154   The remaining filter residue was then digested using a mixture of concentrated nitric acid (HNO_3,
155   1 mL) and concentrated hydrofluoric acid (HF, 0.25 mL) at 120°C for 12 hours (Perron et al.,
156   2020a). The sum of all three steps in the protocol provided the total concentration data for each
157   lithogenic tracer in aerosols which is used in this study (Perron et al., 2020a). Satisfactory
158   recoveries (>90%) were obtained for Al, Fe and Ti when applying the total metal digestion step of
159   the protocol to two reference materials, the Arizona Test Dust (ATD) (Morton et al., 2013) and
160   the GeoPT13 certified Koeln loess (International Association of Geoanalysts) (Potts et al., 2003)
161   (supplementary Table S1). A smaller recovery of 87% (using only certified reference material)
162   obtained for Th highlights the unique extraction and stability chemistry of the metal which our
163   protocol is not optimised for. Thorium concentrations are therefore likely to be slightly
164   underestimated in this study as discussed in section 3. Only total metal concentrations are
165   discussed in the present study.

166

167   2.3 Atmospheric deposition flux estimates
168   The total concentration of each lithogenic tracer in our samples was used to calculate single tracer-
169   dust deposition flux estimates. Additional measurements on the collected aerosols (e.g.; carbon

170 and major ion analysis) were not available for this study, so intrinsic calculation of the total aerosol

171 mass on each individual aerosol filter using these parameters was not possible.

172 In addition, due to the lack of necessary meteorological data to estimate particle deposition

173 velocities specific to our study site, a single coarse particle deposition velocity of 0.2 cm s^{-1} was

174 applied to trace metal-bearing dust deposition estimates based on the literature in similar study

175 regions (Baker et al., 2017; Perron et al., 2020b; Winton et al., 2015). In this study, "$F_{(X)}$" denotes

176 the deposition flux estimate for the individual lithogenic tracer "X". $F_{(X)}$ (in mg m^{-2} d^{-1}) was

177 obtained following equation (1):

178 $$F_{(X)} = C_x \times V_d$$ Eq. (1)

179 where X is the lithogenic tracer – Al, Fe, Th or Ti ; C_x is the total metal concentration (ng m^{-3}) in

180 aerosols and V_d is a constant deposition velocity of 1723 m d^{-1} (0.2 cm s^{-1}). It should be mentioned

181 that a factor of 3 uncertainty was previously attributed to the use of a set deposition velocity as it

182 does not account for specific particle size in different aerosol samples or for specific atmospheric

183 conditions such as humidity and wind speed at the collection time (Baker et al., 2016; Winton et

184 al., 2016; Duce et al, 1991).

185

186 Similar to other studies reported in the literature, a single-tracer dust (lithogenic) deposition flux

187 estimate, $F_{Lith(X)}$, was calculated by dividing $F_{(X)}$ by the average abundance ($[X]_{UCC}$, wt%) of the

188 element X in the UCC as reported in McLennan (2001); Al = 8.04%, Fe = 3.5%, Th = 1.07x10^{-3}%, Ti = 0.41% following equation (2).

189

190 $$F_{Lith(X)} = \frac{F(X) \times 100}{[X]UCC}$$ Eq. (2)

191 While $F_{Lith(X)}$ estimates are solely based on the analysis of a single lithogenic tracer, a multi-tracer

192 dust deposition flux estimate, F_{LithAv}, was obtained by calculating the average of all four $F_{Lith(X)}$

193 (equation 3, N=4) for each individual aerosol sample.

194 $$F_{LithAv} = \frac{\sum F_{Lith(X)}}{N}$$ Eq. (3)

195 Multi-tracer F_{LithAv}, estimates were calculated using both the reported average UCC composition

196 (McLennan, 2001) and Australian soil measurements (see section 2.4 in this study) as references

197 for comparison.

198

199 2.4 Soil sampling and processing

200   Eleven topsoil (0-10 cm) samples were selected from the National Geochemical Survey of

201   Australia (NGSA) Project: Geochemical Atlas of Australia (Geoscience Australia), a continental-

202   scale geochemical survey covering most of Australia (Caritat and Cooper, 2011; Caritat, 2022).

203   In this study, soil samples originating from the southern part of Western Australia, from South

204   Australia and from Victoria were selected and analysed (Figure 1) as they likely better represent

205   particles entrained through the south-east Australian dust path towards our sampling station and

206   the Southern Ocean (Baddock et al., 2015, Supplementary Figure S1). These sources include the

207   geological basins of kati thanda/Lake Eyre and dhungala-barka/Murray-Darling, It should be

208   mentioned that no sample from New South Wales was used for this study although a large part of

209   the dhungala-barka/Murray-Darling basin is located in this state.

210

211   Ten milligrams of each soil sample was dry sieved through a 63 µm nylon screen to capture the

212   soil fraction fine enough to be entrained into the atmosphere (Strzelec et al., 2020a). The sieved

213   fraction was then processed through the same sequential leaching method described in section 2.2

214   (Perron et al., 2020a). Aerosol and soil leachates were analysed for a suite of elements, including

215   Al, Fe, Th and Ti, by Sector Field Inductively Coupled Plasma Mass Spectrometry (HR-ICP-MS,

216   Thermo Fisher Scientific, Element 2) at the Central Science Laboratory of the University of

217   Tasmania. Increased spectral resolution was employed to resolve major spectral interference

218   overlaps associated with analysis of Al, Fe and Ti. Further details on the ICP-MS analysis

219   procedure are provided in Perron et al. (2020a).

220

221   2.5 Atmospheric source tracking

222   The ratio between the total concentration of each lithogenic tracer of interest, T(X), and the total

223   Al concentration, T(Al), in individual aerosol samples was calculated and compared to the same

224   ratio in the average UCC reported in McLennan (2001) and in the average topsoil from

225   southeastern Australia (Section 2.3). The so-called enrichment factor (EF, equation 4) was used to

226   ascertain the lithogenic origin of Fe, Th and Ti in this study.

$$EF = \frac{\frac{C_x}{C_{Al}} aerosol}{\frac{C_x}{C_{Al}} UCC}$$ Eq. (4)

228   Using this approach, an EF value below 10 was considered to indicate a prevailing lithogenic

229   source origin for the metal tracers, while an EF exceeding the threshold value of 10 is associated

with an enrichment from non-lithogenic atmospheric sources such as anthropogenic combustion (Shelley et al., 2015; Perron et al., 2022). Reimann and Caritat (2005) warned about the biases associated with using a low EF threshold to identify anthropogenic sources due to the natural variability in the Earth's crust composition, fractionation of elements during their emission to – and transport within – the atmosphere, and biogeochemical processes during and after aeolian transport. Here, a high EF threshold of 10 is adopted to account for such variability.

3. Results and discussion
3.1 Evaluating the lithogenic origin of the four tracers in aerosols
Enrichment Factors (EF) were calculated for Fe, Th and Ti measured in aerosols, and compared to the Australian soil samples selected from the NGSA (this study) and compared to averaged UCC composition from McLennan (2001) (Table 1). Calculated EF values were used to discard significant contributions of non-lithogenic sources to our lithogenic tracers in kunanyi/Mt Wellington aerosols as indicated by EF>10.

Table 1. Comparison of mean Al, Fe, Th and Ti concentrations measured (ppm) in Australian soil samples (n = 11) compared to concentrations reported in the average UCC by McLennan (2001). Enrichment factors (EFs) calculated for Fe, Th and Ti (using Al as a reference) in aerosols collected at kunanyi/Mount Wellington (n = 125) are also displayed using both crustal references

	UCC	Australian soils		kunanyi/Mount Wellington aerosols	
Al	80400	38560		/UCC	/Australian soil
Fe	35000	22616	**EF(Fe)**	1.6 ± 0.6	1.2 ± 0.5
Th	10.7	10.3	**EF(Th)**	1.3 ± 2.5	0.7 ± 1.2
Ti	4100	4313	**EF(Ti)**	1.2 ± 0.6	0.6 ± 0.6

Overall, EFs close to 1 were measured for all aerosol samples, suggesting that the lithogenic tracers used in this study are indeed of a prevailing crustal origin. Using Australian soil concentration (Table 1 and supplementary Table S2) to calculate EFs resulted in values further away from the threshold of 10. In particular, EFs calculated using Australian soil data are closer to 1 for Fe and Th when compared to using average UCC values (McLennan, 2001). Indeed, underestimated Th measurements due to incomplete sample digestion (section 2.2) in our study result in a similar

252 underestimate of EF. Elemental ratio of Ti/Al in aerosol samples collected at kunanyi/Mt
253 Wellington (Figure 2) were closer to the average ratio of the UCC, resulting in EF(Ti) closer to 1
254 when compared to using average Australian soil measurement as a reference.
255
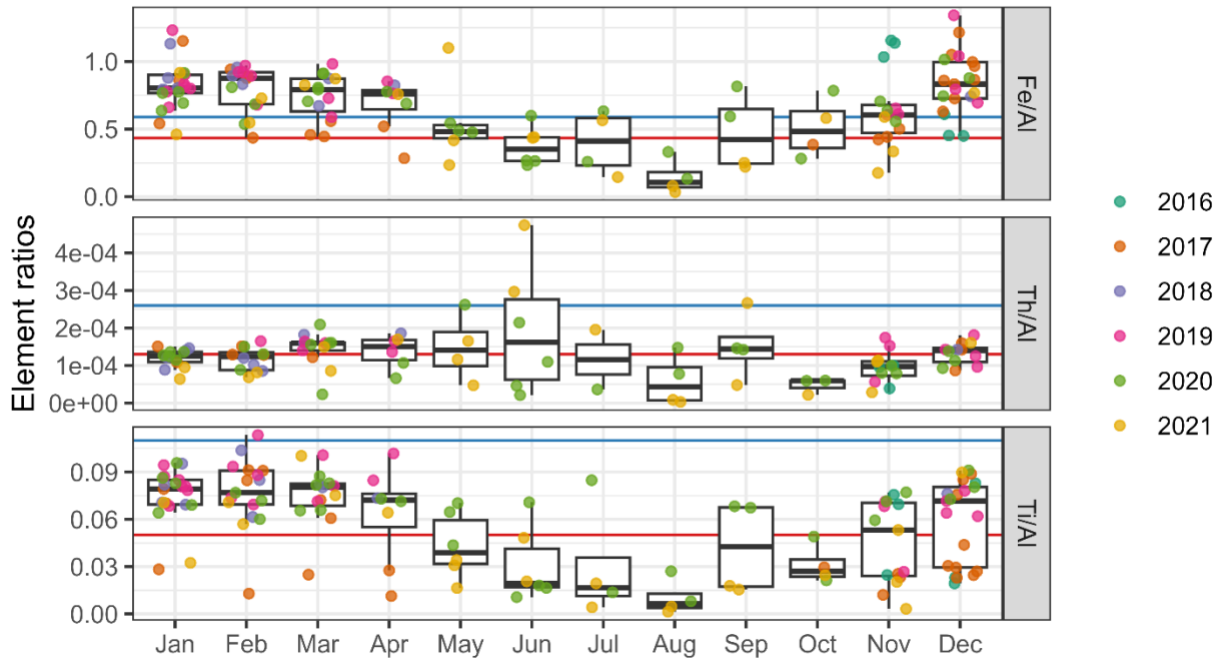
256
257 **Figure 2.** Boxplot of elemental ratios of Fe/Al (top), Th/Al (middle), and Ti/Al (bottom) in kunanyi/ Mt
258 Wellington aerosol samples collected between 2016 – 2021, grouped according to month. Whiskers
259 represent 1.5 times the interquartile range ($75^{th} - 25^{th}$ percentile) beyond the boxes, while the upper, middle,
260 and lower horizontal lines of the box represent the higher interquartile, median value and lower interquartile
261 of the average monthly dataset, respectively. Colours represent each sample collection year. Horizontal red
262 lines represent metal ratios in the average UCC (McLennan, 2001). Horizontal blue lines represent average
263 metal ratios in the eleven selected NGSA Australian soil samples (this study). Two Th outliers (May and
264 June 2020) were excluded from the Th dataset and subsequent calculation for clarity.
265
266 Mean Al and Fe concentrations measured in our Australian soil samples were both twice smaller
267 than the average UCC values reported by McLennan (2001) while Ti and Th concentrations were
268 similar within 10% (Figure 2 and supplementary Table S2). While Australian soil is known for its
269 high Fe content (Mahowald et al., 2019, Strzelec et al., 2020a), a high soil heterogeneity across
270 this vast country may explain such surprising observation. This resulted in calculated Th/Al and
271 Ti/Al ratios higher for Australian soil samples while Fe/Al ratios remained similar compared to
272 the average UCC.
273

274 Elemental ratios calculated for individual aerosol samples are summarised in the supplementary
275 Table S4. Both Fe/Al and Ti/Al ratios showed a clear seasonal trend, with higher ratios resembling
276 mean ratios measured in Australian soil samples (Fe/Al=0.59 and Ti/Al=0.11, Figure 2) in the
277 summertime (December-February) and lower Fe/Al and Ti/Al ratios closer to the average UCC
278 ratios (Fe/Al=0.435 and Ti/Al=0.05, McLennan, 2001) in wintertime (June-August, Figure 2).
279 Summertime Fe/Al ratios in kunanyi/Mt Wellington aerosols were slightly higher (Fe/Al =0.72)
280 than the Australian soil measurements. This can be explained by increased contribution of local
281 soil emission from Tasmania under drier weather conditions as the NGSA database shows higher
282 Fe/Al ratio (on average 0.7, n=21 samples) in Tasmanian soil compared to other soil across
283 Australia (Caritat and Cooper, 2011; Caritat, 2022). While enhanced air-masses originating from
284 the Australian mainland cannot be observed in the summertime using HYSPLIT model
285 (supplementary Figure S1), the Australian Bureau of Meteorology reports increasing southwards
286 blowing winds at our sampling station from January through to March (supplementary Figure S2).
287 Such discrepancies emphasise the complex regional wind pattern influencing our sampling station
288 and highlight the need to consider other parameters such as seasonal changes in environmental
289 conditions at the source region when investigating aerosol entrainment and transport. Ti/Al ratios
290 were found to lie between our Australian soil (Ti/Al = 0.11) and UCC (Ti/Al = 0.05) references
291 from December through to May, then falling below the UCC ratio in the cooler months of the year.
292 This monthly variability indicates different lithogenic sources of Fe and Ti are likely to influence
293 the atmospheric loading at our sampling station throughout the year. The onset of the dust season
294 on the Australian mainland (October-November, Baddock et al., 2015) may explain part of the
295 summer (dusty) season atmospheric inputs at our kunanyi /Mt Wellington aerosol sampling station,
296 as evidenced by higher Fe/Al (and Ti/Al) ratios in aerosols. On the other hand, other atmospheric
297 sources (locally derived from Tasmania or from long-range transport over the Southern Ocean)
298 with a similar (lower) metal/Al signature than the UCC seem to prevail in our study region during
299 winter. However, the small number of aerosol samples available between May - October in our
300 study does not allow for accurate assessment of trends during the winter period. Much smaller
301 variability was observed for the Th/Al ratio calculated in kunanyi/Mt Wellington aerosols (mean
302 Th/Al = 0.00017) across the time-series, with an overall median ratio close to that of the UCC
303 (mean Th/Al = 0.00013) across most of the year except during August and October.

304

305 Differences between elemental ratios in soil and in aerosol samples may stem from atmospheric
306 processes occurring during transport between source regions and the sampling site including the
307 preferential settling of denser (e.g., oxyhydroxides) minerals over lighter minerals (e.g., clay), and
308 from the mixing of different lithogenic air-masses during atmospheric transport. Analysis of a
309 large set of soil samples, including more locations across Australia and particularly in Tasmania,
310 as well as high resolution information on wind speed and direction at the sampling site and for the
311 duration of the timeseries is necessary to better assess the relative contribution of different
312 Australian dust sources to the lithogenic particulate loading at kunanyi/Mount Wellington.

313

314 3.2 Single tracer lithogenic particle fluxes at kunanyi/Mount Wellington: characteristics
315 and trends
316 Thorium and Ti are commonly used as tracers of lithogenic atmospheric deposition fluxes as they
317 are almost exclusively derived from lithogenic material and have little reactivity or biological
318 utility in the atmosphere (Boës et al., 2001; Ohnemus and Lam, 2015). While Al may be emitted
319 to the atmosphere by anthropogenic sources, its prevailing source in the offshore atmosphere
320 remains crustal material (Xu and Weber, 2021). Although Fe solubility vary following physico-
321 chemical processes during the atmospheric transport, the soluble Fe fraction remains small
322 compared to the total (mostly refractory) fraction of Fe delivered by dust. Hence, if all four tracers
323 have a unique lithogenic source, the use of a multiple tracer lithogenic flux estimate can reduce
324 the uncertainty associated with the variability of a single metal's concentration due to
325 contamination, deviation from the UCC or secondary atmospheric inputs (Traill et al., 2022).

326

Table 2. Correlation coefficient (R^2) between tracer concentrations in
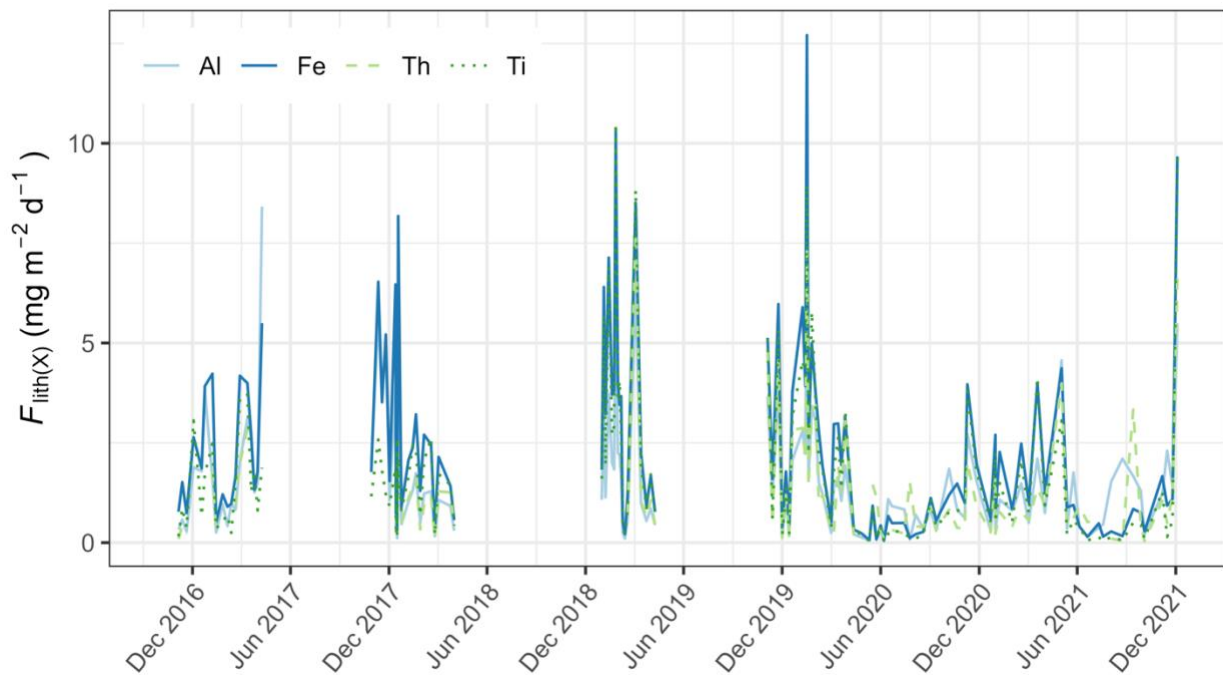kunanyi/Mount Wellington aerosols.

	Al	Th	Fe	Ti
Al	1	-	-	-
Th	0.90	1	-	-
Fe	0.87	0.82	1	-
Ti	0.74	0.84	0.83	1

327

328 A strong correlation (mostly $R^2 > 0.8$) was found between the total atmospheric concentrations of
329 Al, Fe, Th and Ti in the individual samples (Table 2). The strongest correlation ($R^2 = 0.90$) was
330 found between Al and Th and the weakest correlation ($R^2 = 0.74$) was found between total Ti and

331 Al concentrations in aerosols. Such strong correlations suggest that a common prevailing source

332 may supply all four tracers to kunanyi/Mt Wellington sampling station. Australian soil samples

333 collected in the state of Victoria and analyzed in this study also showed a good correlation between

334 the four lithogenic tracers, with R^2 of 0.97, 0.74 and 0.73 for Fe, Th and Ti when compared to Al

335 (based on Table S4 data). Such correlation was not found for soil samples from South Australia

336 (only 2 soil samples from Western Australia). However, the small number of soil sample analysed

337 in this study (n=4 for Victoria and n=5 in South Australia)) is not sufficient to draw conclusion on

338 the potential origin of metals in kunanyi/Mt Wellington aerosol samples. The NGSA database

339 available from Caritat and Cooper (2011) also shows a strong correlation (>0.70) between Fe and

340 Al measurements in soil samples from New South Wales, South Australia and Tasmania using an

341 aqua regia mineralization and x-ray florescence analysis protocol.

342

343
344 **Figure 3.** Individual tracer flux, $F_{Lith(X)}$ (mg m^{-2} d^{-1}), at the kunanyi/Mount Wellington aerosol sampling
345 station from 2016 to 2021. Data points represent each aerosol mid-sampling period. Gaps in the time series
346 are periods where samples were not collected due to logistical limitations (winters) or instrument
347 maintenance. Here, $F_{Lith(X)}$ are calculated using the average UCC content for each metal as reported in
348 McLennan (2001).

349

350 Dust deposition fluxes estimated using individual tracer (Al, Fe, Th, and Ti) concentrations

351 measured in kunanyi/Mount Wellington aerosols, called $F_{Lith(X)}$, showed similar variability

352 throughout the time-series (2016-2021, Figure 3). Overall, the smallest $F_{Lith(Th)}$ flux was estimated

353   using Th as a single lithogenic tracer, ranging between 0.03 and 7.8 mg m^{-2} d^{-1}. The largest dust

354   flux was obtained using Fe as a lithogenic tracer and ranged between 0.05 and 12.7 mg m^{-2} d^{-1}

355   ($F_{Lith(Fe)}$, Figure 3). Lithogenic flux estimates calculated using Al and Ti concentrations in aerosols

356   ranged from 0.06 - 8.4 mg m^{-2} d^{-1} and from 0.03 - 10.5 mg m^{-2} d^{-1}, for $F_{Lith(Al)}$ and $F_{Lith(Ti)}$,

357   respectively. Despite slight differences found between $F_{Lith(X)}$ estimates obtained using different

358   lithogenic tracers, the magnitude of the difference between the highest and lowest $F_{Lith(X)}$ estimates

359   varied by only a factor of 2, which reinforces the likelihood of a common prevailing atmospheric

360   source for all four tracers.

361

362   This finding corroborates work presented by Traill et al. (2022), where concentrations of all four

363   lithogenic tracers showed similar variabilities in marine sinking particles collected in the

364   subantarctic region of the Southern Ocean south of Tasmania (SOTS station). Similarly, Traill et

365   al. (2022) estimated higher lithogenic fluxes when using Fe as a lithogenic tracer and lower

366   lithogenic fluxes when using Th as a lithogenic tracer (Traill et al., 2022). Median $F_{Lith(X)}$ estimates

367   measured at the kunanyi/Mt Wellington sampling site (this study: 1.2, 1.7, 0.8 and 1.1 mg m^{-2} d^{-1}

368   using Al, Fe, Th and Ti as individual lithogenic tracer, respectively) compares well with reported

369   dust deposition fluxes of 1.4 - 5 mg m^{-2} d^{-1} estimated by models in the study region (Jickells et al.,

370   2005; Mahowald et al., 2005; Weis et al., 2024) and other Southern Hemisphere dust fluxes <2.7

371   mg m^{-2} d^{-1} reported off the coasts of South Africa and South America, away from major dust

372   sources (Menzel Barraqueta et al., 2019). Our flux estimates are smaller than mineral dust

373   deposition estimates of 4.0 - 25.0 mg m^{-2} d^{-1} (based on Ti concentration in aerosols) reported by

374   Strzelec et al. (2020a) in Western Australia, much closer to large Australian deserts.

375

376   Overall, maximum $F_{Lith(X)}$ estimates in our study were calculated during austral summer months

377   (roughly December – March). Different metals are observed to dominate the summer $F_{Lith(X)}$ peak

378   each year, with Al showing the highest $F_{Lith(X)}$ flux in summer 2016/17 (8.4 mg m^{-2} d^{-1}), Fe in

379   2017/18 (8.2 mg m^{-2} d^{-1}) and in 2019/20 (12.7 mg m^{-2} d^{-1}), and Ti in 2018/19 (10.5 mg m^{-2} d^{-1})

380   and in 2021/22 (9.6 mg m^{-2} d^{-1}). This may be due to variabilities in the nature and composition of

381   the dominant dust source arriving at the sampling site each year, including the impact of dust-

382   containing fire emissions during the summer seasons 2018/19 and 2019/20 (Perron et al. 2022).

383

384   3.3 Multi tracer particle flux

385   All four tracers (Al, Fe, Th, and Ti) measured in kunanyi/Mount Wellington aerosols showed a

386   strong correlation with one another and a similar variability over time (section 3.1), suggesting

387   that they originated from a single terrestrial source. This supports the approach taken in this study

388   whereby a multi-tracer lithogenic deposition flux, called F_{LithAv}, is estimated by averaging $F_{Lith(X)}$

389   fluxes obtained using each of the four tracers for each sample. The resulting F_{LithAv} estimated at

390   our station between 2016 and 2021 is displayed in Figure 4 and provides a more robust estimate

391   of deposition flux by smoothing variability between tracers (displayed in Figure 3). Individual and

392   average lithogenic flux estimates ($F_{Lith(X)}$ and F_{LithAv}, respectively) calculated in this study are

393   summarised for individual samples in the supplementary Tables S5 and S6, respectively.

394

395
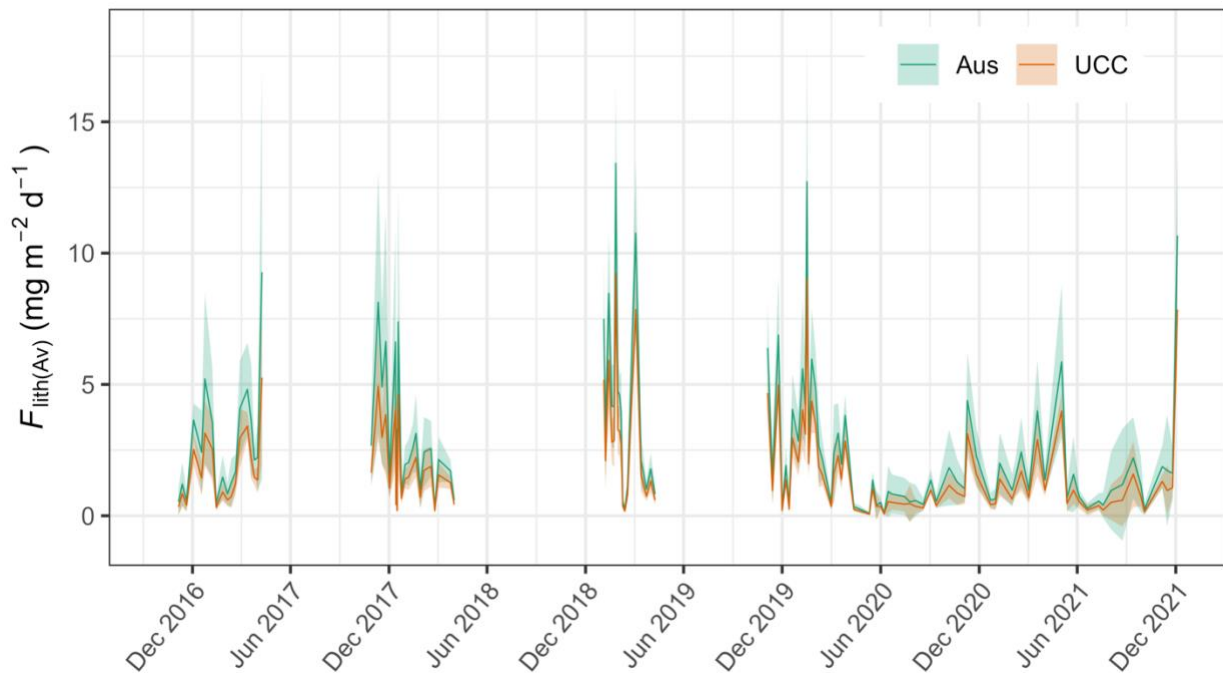
Figure 4. Multi-tracer lithogenic flux estimate, F_{LithAv}, expressed in mg m^{-2} d^{-1}, corresponding to the
average of all individual tracer fluxes ($F_{Lith(X)}$) calculated based on the lithogenic composition of the UCC
(orange colour) and that of the eleven Australian soil samples measured in this study (green colour) .
Shadings represent +/- one F_{LithAv} standard deviation of the average (solid lines).

400

401   A mean F_{LithAv} value of 1.8 ± 1.3 mg m^{-2} d^{-1} was calculated based on the analysis of aerosol samples

402   collected between 2016 and 2021 at kunanyi/Mt Wellington (Tasmania, Figure 4 orange colour).

403   Throughout our time series, the highest F_{LithAv} values were observed in January 2019 and 2020,

404   with flux peaks reaching 9.2 in January 2019 and 9.0 mg m^{-2} d^{-1} in January 2020, respectively.

405   Noticeable peak fluxes of 7.9 mg m^{-2} d^{-1} also occurred in early March 2019 and in mid-December

406   2021. Extended periods of low F_{LithAv} estimates (≦0.5 mg m^{-2} d^{-1}) were observed during the two

407   austral winter periods sampled, with a minimum flux of 0.06 mg m^{-2} d^{-1} reached in May 2020

408   (Figure 4). There is therefore an apparent seasonal trend in dust deposited at the kunanyi/Mt

409   Wellington site, with higher F_{LithAv} observed in warmer periods (November - March) and lower

410   fluxes in cooler periods of the year (May - August). It should be mentioned that a mean F_{LithAv}

411   value of 2.7 ± 1.9 mg m^{-2} d^{-1} is estimated when using the average metal content in Australian soil

412   analyzed in this study (Figure 4 green colour). Indeed, while Th and Ti contained in our eleven

413   Australian soil samples show similar concentrations (within 10%) as in the average UCC

414   (McLennan, 2001), Al and Fe concentrations in these local soil samples differ by 52 and 35%,

415   respectively. This result in higher F_{LithAv} estimated using Australian soil data (Figure 4).

416   The mean F_{LithAv} observed in this study, of 1.8 mg m^{-2} d^{-1} when using the average UCC and 2.7

417   mg m^{-2} d^{-1} when using the average Australian soil measurement (Table S5), fall within the dust

418   deposition range of 1.1 - 5.5 mg m^{-2} d^{-1} reported by models in southeastern Australia, which

419   account for soil erodibility, soil particle size distribution and wind friction velocity (Albani et al.,

420   2014; Weis et al., 2024). In the Southern Ocean south of Tasmania, smaller mineral dust fluxes of

421   0.37 mg m^{-2} d^{-1} and 1.0 mg m^{-2} d^{-1} were reported based on aerosol Fe measurements at sea, particle

422   size and surface wind speed (Bowie et al., 2009) and based on Al, Fe, Th and Ti measurements in

423   marine sinking particles (Traill et al., 2022), respectively. Traill et al. (2022) reported a similar

424   annual variability in lithogenic deposition flux at SOTS between 2011 and 2018, with minimum

425   F_{LithAv} around 0.5 mg m^{-2} d^{-1} in July-September and an earlier dust deposition peak (compared to

426   our study) in November-December, up to 2.5 mg m^{-2} d^{-1}. Strzelec et al. (2020a) also reported (up

427   to 6 times) higher mineral dust fluxes in warmer months compared to cooler months based on Ti

428   analysis in aerosols from Western Australia. In particular, the two summer seasons showing F_{LithAv}

429   over 9.0 mg m^{-2} d^{-1} correspond to large bushfire seasons in Tasmania and in Australian mainland

430   upwind from Tasmania, respectively (Perron et al., 2022). Indeed, fire events are known to

431   exacerbate dust entrainment into the atmosphere both during (pyro convective updrafts) and post

432   (burnt ground) fire event (Hamilton et al., 2022). It is worth noting that F_{LithAv} estimated using

433   Australian soil measurements (this study) fall closer to the mean reported estimate found in the

434   literature while using the average UCC value result in lower-end F_{LithAv} estimate compared to the

literature. While F_{LithAv} estimated using the average UCC may present an advantage in being more comparable with other studies worldwide, F_{LithAv} estimated using Australian soil data may be more relevant for validating model outputs as it likely better represents true deposition fluxes in our study region. Overall, the choice of one or the other crustal source result in up to a factor 2 difference in the calculated $F_{LithAv.}$
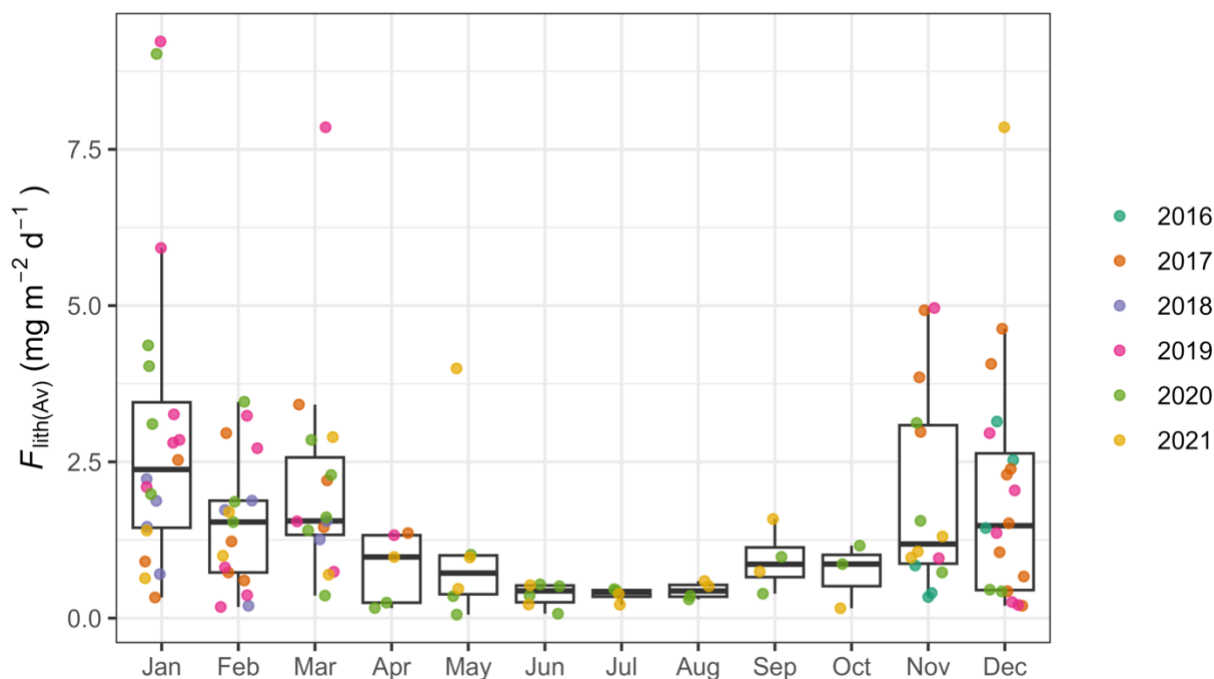
Figure 5. Monthly F_{LithAv} estimates, in mg m^{-2} d^{-1}, based on lithogenic tracer analysis in aerosol samples collected between 2016-2021 at the kunanyi/Mt Wellington site. Individual (weekly) samples are shown as dots and the colour code represents each collection year. Whiskers represent 1.5 times the interquartile range (75th – 25th percentile) beyond the boxes, while the upper, middle, and lower horizontal lines of the box represent the higher interquartile, median value and lower interquartile of the average monthly dataset, respectively.

Greatest F_{LithAv} fluxes are annually observed during the austral summer (December - March), with median F_{LithAv} of 2.4 mg m^{-2} d^{-1} in January and around 1.4 mg m^{-2} d^{-1} in December, February and March across all years (Figure 5). This tendency aligns with higher frequency of dust storms occurring in Australia's main geological basins during warmer months (late austral spring and summer), resulting in higher dust deposition fluxes (O'Loingsigh et al., 2017). The summers of 2017/2018 (Nov-Dec), 2018/19 (Jan-Feb) and 2019/20 (Dec-Feb) had especially high F_{LithAv} fluxes compared to other summer periods in the time-series (Figure 5). These observations are consistent with the year 2017 being identified as the third driest year since

455 records have been kept in Australia (Steffen et al., 2018), and the two following summer periods

456 being identified as strong bushfire years, across Tasmania in 2018/2019, and across southeast

457 Australia in 2019/2020 (Perron et al., 2022). Relatively smaller peaks were observed during the

458 summer of 2020/21 and, to a lesser extent, during the 2016/17 summer (Figure 5). This may

459 reflect two wetter summer periods under the influence of El Niño Southern Oscillation positive

460 phase (La Niña), where increased moisture in the topsoil restricted particles from being eroded

461 and entrained by air masses (Bureau of Meteorology, 2022). In addition, fewer bushfire

462 emissions during these two wetter summer periods may have resulted in less dust emissions due

463 to increased vegetation cover on the soil (Bureau of Meteorology, 2022). Wetter summer seasons

464 may also explain a shift in F_{LithAv} peaks towards the end of the summer seasons 2016/17 and

465 2020/21 (February - March) compared to the December-January F_{LithAv} peak observed in

466 2017/18, 2018/19, and 2019/20 (Figure 5).

467

468   4. Conclusions

469 This study explores the seasonal and interannual variability of the lithogenic deposition flux using

470 analysis of Al, Fe, Th, and Ti (as lithogenic tracers) in aerosol samples collected at kunanyi/Mt

471 Wellington (Tasmania, Australia). Enrichment factors close to 1 and elemental ratios similar to

472 those measured in soil samples collected in Australian dust source regions confirmed the crustal

473 origin of all four tracers. Deposition fluxes, $F_{Llith(X)}$, calculated using each tracer individually

474 showed small differences, of a factor 2 on average, between one another throughout the 2016-2021

475 time series. This study suggests the use of a multi-tracer (averaged) dust deposition flux estimate

476 as a more robust method to account for variability of individual tracers in aerosols.

477 The mean F_{LithAv} of 1.8 mg m^{-2} d^{-1} calculated in this study across the 2016-2021 time-series is

478 consistent with earlier lithogenic deposition fluxes reported in the literature. Dust flux maxima (up

479 to 9.2 mg m^{-2} d^{-1}) were consistently observed during the austral summer, while minimum annual

480 F_{LithAv} (down to 0.06 mg m^{-2} d^{-1}) were estimated in the winter. Overall, individual year F_{LithAv}

481 fluxes aligned well with the occurrence of known dust and bushfire events in the summertime as

482 well as other global meteorological events such as El Niño Southern Oscillation (ENSO) which

483 drive the weather patterns across southeast Australia.

484 Dust deposition fluxes calculated in this study hold some uncertainties of a factor 3 and a factor 2
485 due to the use of a set deposition velocity and the assumption of metal abundance as per the average
486 UCC, respectively. While using the averaged UCC to calculate F_{LithAv} may present an advantage
487 in being more comparable with other studies worldwide, we show that F_{LithAv} estimates (0.09 –
488 13.4 mg m^{-2} d^{-1}) calculated using metal abundance in Australian soils are in better agreement with
489 dust fluxes reported by global models in our study region. Therefore, understanding local soil
490 composition is essential to estimating dust deposition fluxes in different study regions. Overall,
491 the uncertainty in field-based dust deposition flux estimates likely remain smaller than
492 uncertainties associated with model parametrization.

493 As dust deposition is now being recognized as a major source of vital micro-nutrients such as Fe
494 to the Southern Ocean, accurately quantifying dust fluxes is vital to understanding primary
495 production in the Southern Ocean and how this may change under future climate scenarios. Our
496 observed dust flux maxima in austral summer may also provide a much-needed regional pulse of
497 nutrients to phytoplankton when water column nutrients are being depleted through the growing
498 season. Additional observations covering a wider geographical area and greater temporal coverage
499 (including time-series stations and winter sampling periods) are required to better constrain
500 seasonal and interannual variability. Our study adds vital data to the relatively few field-based dust
501 deposition flux estimates available to validate model outputs, especially for Southern hemisphere
502 dust sources (including Australia) which greatly vary in nature and composition.
503

Author contributions
505 A.R.B. was responsible for project conceptualisation, funding acquisition, resources and
506 supervision. M.M.G.P. was responsible for part of the sample collection, sample processing, data
507 interpretation, processing and curation as well as for manuscript drafting. S.M was responsible for
508 part of the sample collection and analysis, and for laboratory supervision. T.H was responsible for
509 data curation. C.N was responsible for the analysis of soil samples. C.H was responsible for part
510 of the sample collection, sample processing, data curation and the original draft writing. A.T. was
511 responsible for instrumental analysis. P.dC. was responsible for part of the sample collection and
512 data curation. M.S. was responsible for part of the sample collection and sample processing. All

513 authors were responsible for data interpretation and validation and reviewing and editing the
514 manuscript.
515

Competing interest

518

Code/ Data availability

519 Code/ Data availability
520 All data produced in this study is available either in the manuscript or in the supplementary files.
521

Acknowledgements

539

Acknowledgment to country

540 Acknowledgment to country

541 Before the white settlement of lutruwita/Tasmania, kunanyi/Mount Wellington was a prominent

542 feature in the lives of the Moomairremener people for thousands of years and continues to be. We

543 pay our respects to elders' past, present and emerging and are thankful to have been able to study

544 this region.

545

References

547 Albani S, et al. 2014, 'Improved dust representation in the Community Atmosphere Model', *Journal of*
548 *Advances in Modeling Earth Systems*, vol. 6, no. 3, pp. 541–570, doi/10.1002/2013MS000279.

549 Anderson RF, et al. 2016, 'How well can we quantify dust deposition to the ocean?', *Philosophical*
550 *Transactions of the Royal Society A: Mathematical, Physical and Engineering Sciences*, vol. 374, no.
551 2081, p. 20150285, doi/10.1098/rsta.2015.0285.

552 Baddock M, et al. 2015, 'Drivers of Australian dust: a case study of frontal winds and dust dynamics in
553 the lower lake Eyre basin', *Earth Surface Processes and Landforms*, vol. 40, no. 14, pp. 1982–1988,
554 doi.org/10.1002/esp.3773

555 Baker AR, et al. 2016, 'Trace element and isotope deposition across the air–sea interface: progress and
556 research needs', *Philosophical Transactions of the Royal Society A: Mathematical, Physical and*
557 *Engineering Sciences*, vol. 374, no. 2081, p. 20160190, doi/10.1098/rsta.2016.0190.

558 Baker AR, et al. 2017, 'Observation- and model-based estimates of particulate dry nitrogen deposition to
559 the oceans', *Atmospheric Chemistry and Physics*, vol. 17, no. 13, pp. 8189–8210, doi.org/10.5194/acp-17-
560 8189-2017.

561 Baker AR, Li M and Chance R, 2020, 'Trace Metal Fractional Solubility in Size-Segregated Aerosols
562 From the Tropical Eastern Atlantic Ocean', *Global Biogeochemical Cycles*, vol. 34, no. 6, p.
563 e2019GB006510, doi/10.1029/2019GB006510.

564 Bindu G, et al. 2016, 'Pattern of aerosol mass loading and chemical composition over the atmospheric
565 environment of an urban coastal station', *Journal of atmospheric and solar-terrestrial physics*,
566 vol. 138, 10.1016/j.jastp.2016.01.004

567 Bowie AR, et al. 2009, 'Biogeochemical iron budgets of the Southern Ocean south of Australia:
568 Decoupling of iron and nutrient cycles in the subantarctic zone by the summertime supply', *Global*
569 *Biogeochemical Cycles*, vol. 23, no. 4, doi/10.1029/2009GB003500.

570 Bowler JM, 1976, 'Aridity in Australia: Age, origins and expression in aeolian landforms and sediments',
571 *Earth-Science Reviews*, vol. 12, no. 2–3, pp. 279–310, doi.org/10.1016/0012-8252(76)90008-8.

572 Bureau of Meteorology 2022, *ENSO Outlook*, www.bom.gov.au/climate/enso/outlook.

573 Caritat P de and Cooper M, 2011, *National Geochemical Survey of Australia: The Geochemical Atlas of*
574 *Australia*, dx.doi.org/10.11636/Record.2011.020.

575 de Caritat P de, 2022, 'The National Geochemical Survey of Australia: review and impact',
576 *Geochemistry: Exploration, Environment, Analysis,* vol. 22, geochem2022-032,
577 doi.org/10.1144/geochem2022-032.

578 Crawford J, et al. 2021, 'Fingerprinting Australian soils based on their source location', *Atmospheric*
579 *Pollution Research*, vol. 12, no. 3, pp. 173–183, doi.org/10.1016/j.apr.2021.01.007.

580   Cudahy T, et al. 2016, 'Satellite-derived mineral mapping and monitoring of weathering, deposition and
581   erosion', *Scientific Reports*, vol. 6, p. 23702, doi.org/10.1038/srep23702.

582   Cutter G, et al. 2017, 'Sampling and Sample-handling Protocols for GEOTRACES Cruises', Version 3.0.

583   De Deckker P, 2019, 'An evaluation of Australia as a major source of dust', *Earth-Science Reviews*, vol.
584   194, pp. 536–567, doi.org/10.1016/j.earscirev.2019.01.008.

585   Duce RA, et al. 1991, 'The atmospheric input of trace species to the world ocean', *Global*
586   *Biogeochemical Cycles*, vol. 5, no. 3, pp. 193–259, doi/10.1029/91GB01778.

587   Hamilton DS, et al. 2022, 'Earth, Wind, Fire, and Pollution: Aerosol Nutrient Sources and Impacts on
588   Ocean Biogeochemistry', *Annual Review of Marine Science*, vol. 14, no. 1, pp. 303–330,
589   doi/10.1146/annurev-marine-031921-013612.

590   Ito A, et al. 2020, 'Evaluation of aerosol iron solubility over Australian coastal regions based on inverse
591   modeling: implications of bushfires on bioaccessible iron concentrations in the Southern Hemisphere',
592   *Progress in Earth and Planetary Science*, vol. 7, no. 1, p. 42, doi.org/10.1186/s40645-020-00357-9.

593   Jickells T, et al. 2005, 'Global Iron Connections Between Desert Dust, Ocean Biogeochemistry, and
594   Climate', *Science*, vol 308, p. 67-71, doi/10.1126/science.1105959.

595   Mackie DS, et al. 2008, 'Biogeochemistry of iron in Australian dust: From eolian uplift to marine
596   uptake', *Geochemistry, Geophysics, Geosystems*, vol. 9, no. 3, doi/10.1029/2007GC001813.

597   Mahowald NM, et al. 2005, 'Atmospheric global dust cycle and iron inputs to the ocean', *Global*
598   *Biogeochemical Cycles*, **19**(4), GB4025. doi.org/10.1029/2004GB002402.

599   Mahowald NM, et al. 2006, 'Change in atmospheric mineral aerosols in response to climate: Last glacial
600   period, preindustrial, modern, and doubled carbon dioxide climates', *Journal of Geophysical Research:*
601   *Atmospheres*, vol. 111, no. D10, doi/10.1029/2005JD006653.

602   Mahowald NM, et al. 2009, 'Atmospheric Iron Deposition: Global Distribution, Variability, and Human
603   Perturbations', *Annual Review of Marine Science*, vol. 1, no. 1, pp. 245–278,
604   doi/10.1146/annurev.marine.010908.163727.

605   McLennan SM, 2001, 'Relationships between the trace element composition of sedimentary rocks and
606   upper continental crust', *Geochemistry, Geophysics, Geosystems*, vol. 2, no. 4,
607   doi/10.1029/2000GC000109.

608   Menzel Barraqueta J-L, et al. 2019, 'Atmospheric deposition fluxes over the Atlantic Ocean: a
609   GEOTRACES case study', *Biogeosciences*, 16, doi.org/10.5194/bg-16-1525-2019.

610   Ohnemus DC and Lam PJ, 2015, 'Cycling of lithogenic marine particles in the US GEOTRACES North
611   Atlantic transect', *Deep Sea Research Part II: Topical Studies in Oceanography*, vol. 116, pp. 283–302,
612   doi.org/10.1016/j.dsr2.2014.11.019.

613   O'Loingsigh T, et al. 2017, 'Sources and pathways of dust during the Australian "Millennium Drought"
614   decade', *Journal of Geophysical Research: Atmospheres*, vol. 122, no. 2, pp. 1246–1260,
615   doi/10.1002/2016JD025737.

616   Perron MMG, et al. 2020a, 'Assessment of leaching protocols to determine the solubility of trace metals
617   in aerosols', *Talanta*, vol. 208, p. 120377, doi.org/10.1016/j.talanta.2019.120377.

618   Perron MMG, et al. 2020b, 'Origin, transport, and deposition of aerosol iron to Australian coastal waters',
619   *Atmospheric Environment*, vol. 228, p. 117432, doi.org/10.1016/j.atmosenv.2020.117432.

Perron MMG, et al. 2021, 'Atmospheric inputs of volcanic iron around Heard and McDonald Islands, Southern ocean', *Environmental Science : Atmospheres*, vol 1, p 508-517, doi.org/10.1039/D1EA00054C.

Perron MMG, et al. 2022, 'Trace elements and nutrients in wildfire plumes to the southeast of Australia', *Atmospheric Research*, vol. 270, p. 106084, doi.org/10.1016/j.atmosres.2022.106084.

Reimann C, and P Caritat de. 2005. ' Distinguishing between natural and anthropogenic sources for elements in the environment: regional geochemical surveys versus enrichment factors', *Science of the Total Environment*, vol 337, p 91-107, doi.org/10.1016/j.scitotenv.2004.06.011

Shelley RU, Morton PL and Landing WM 2015, 'Elemental ratios and enrichment factors in aerosols from the US-GEOTRACES North Atlantic transects', *Deep Sea Research Part II: Topical Studies in Oceanography*, vol. 116, pp. 262–272, doi.org/10.1016/j.dsr2.2014.12.005.

Sprigg RC. 1982, 'Some stratigraphic consequences of fluctuating Quaternary sea levels and related wind regimes in southern and central Australia, In: *Quaternary dust mantles, China, New Zealand and Australia'*. Wasson RJ. ed. pp. 211-240. Australian National University: Canberra.

Steffen W, Rice M and Alexander D 2017, 'Another record-breaking year for heat and extreme weather', Climate Council of Australia, ISBN 978-1-925573-47-3.

Strzelec M, et al. 2020a, 'Atmospheric Trace Metal Deposition from Natural and Anthropogenic Sources in Western Australia', *Atmosphere*, vol. 11, no. 5, p. 474, doi.org/10.3390/atmos11050474.

Strzelec M, et al. 2020b, 'Atmospheric Trace Metal Deposition near the Great Barrier Reef, Australia', *Atmosphere*, 11(4), 394, doi.org/10.3390/atmos11040390.

Strzelec M, 2020c, 'Source characterisation of atmospheric trace metal deposition around Australia'. University of Tasmania. Thesis. Doi.org/10.25959/100.00035895.

Traill CD, et al. 2022, 'Lithogenic Particle Flux to the Subantarctic Southern Ocean: A Multi-Tracer Estimate Using Sediment Trap Samples', *Global Biogeochemical Cycles*, vol. 36, no. 9, doi/10.1029/2022GB007391.

Vecchio M.A., et al. 2024, 'Provenance of mineral dust deposited on Antarctica over the last sixty years by strontium isotopic analysis of snow from Dome C', *Atm. Env.*, vol 338, doi:10.1016/j.atmosenv.2024.120850

Weis J, et al. 2022, 'Southern Ocean phytoplankton stimulated by wildfire emissions and sustained by iron recycling', *Geophys. Res. Lett.*, vol. 49, p. 1–11, doi:10.1029/2021gl097538

Weis J., et al. 2024, 'One-third of Southern Ocean productivity is supported by dust deposition', *Nature*, vol 629, pp. 603–608, doi:10.1038/s41586-024-07366-4

Winton VHL, et al. 2015, 'Fractional iron solubility of atmospheric iron inputs to the Southern Ocean', *Marine Chemistry*, vol. 177, pp. 20–32, doi.org/10.1016/j.marchem.2015.06.006.

Winton VHL, et al. 2016, 'Dry season aerosol iron solubility in tropical northern Australia', *Atmospheric Chemistry and Physics*, vol. 16, no. 19, pp. 12829–12848, doi.org/10.5194/acp-16-12829-2016.

Xu H., and Weber T. 2021, 'Ocean dust deposition rates constrained in a data-assimilation model of the marine aluminum cycle', *Global Biogeochemical Cycles*, vol 35 no. 9. doi.org/10.1029/2021GB007049